PHYSICAL REVIEW D **81,** 094036 (2010)

# Next-to-leading-order QCD corrections to graviton production at hadron colliders

Stefan Karg and Michael Krämer
*Institut für Theoretische Physik, RWTH Aachen University, D-52056 Aachen, Germany*

Qiang Li and Dieter Zeppenfeld
*Institut für Theoretische Physik, Karlsruhe Institute of Technology, D-76128 Karlsruhe, Germany*
(Received 25 February 2010; published 28 May 2010)

Models with large extra dimensions predict the existence of Kaluza-Klein graviton resonances. We compute the next-to-leading-order QCD corrections to graviton plus jet hadro-production, which is an important channel for graviton searches at the Tevatron and the LHC. The QCD corrections are sizable and lead to a significant reduction of the scale dependence. We present numerical results for cross sections and distributions, and discuss the uncertainty from parton distribution functions and the ultraviolet sensitivity of the theoretical prediction.

DOI: 10.1103/PhysRevD.81.094036 PACS numbers: 14.70.Kv, 11.10.Kk, 12.38.Bx

## I. INTRODUCTION

The search for new physics at the TeV-scale is one of the major tasks for current and future high-energy physics experiments. Models with extra space dimensions and TeV-scale gravity address the problem of the large hierarchy between the electroweak and Planck scales, and predict exciting signatures of new physics that can be probed at colliders [1].

In the $D = 4 + \delta$ dimensional model proposed by Arkani-Hamed, Dimopoulos and Dvali (ADD) [2], the standard model (SM) particles are constrained to a $3 + 1$ dimensional brane, while gravity can propagate in a $4 + \delta$ dimensional space-time. For simplicity, the additional $\delta$-dimensional space is assumed to be a torus with common compactification radius $R$. In such a model, the four-dimensional effective Planck scale $M_{\mathrm{P}}$ is related to the fundamental scale $M_{\mathrm{S}}$ by [2]

$$M_{\mathrm{P}}^2 = 8\pi R^{\delta} M_{\mathrm{S}}^{\delta+2}. \tag{1.1}$$

For a large compactification radius $R$ it is thus possible that the fundamental scale is near the weak scale, $M_{\mathrm{S}} \sim$ TeV. In the ADD model, deviations from the standard Newton law of gravity are predicted at distances around $R \approx 0.83 \times 10^{-16+30/\delta}$ mm $\times$ (2.4 TeV$/M_{\mathrm{S}})^{1+2/\delta}$. Current terrestrial test of gravity exclude $R \geq 37(44)$ $\mu m$ for $\delta = 2(1)$ [3], which, using Eq. (1.1), translates into $M_{\mathrm{S}} \geq 3.6$ TeV for $\delta = 2$. Further constraints have been derived from astrophysics and cosmology, in particular, for $\delta < 4$, but they can be evaded in specific models [4] and do not lessen the importance of collider searches for extra dimensions.

The $D = 4 + \delta$ dimensional graviton corresponds to a tower of massive Kaluza-Klein (KK) modes in four dimensions. The interaction of these spin-2 KK gravitons with SM matter can be described by an effective theory [5–7] with the Lagrangian

$$\mathcal{L}_{\mathrm{int}} = -\frac{1}{\bar{M}_{\mathrm{P}}} \sum_{\vec{n}} G_{\mu\nu}^{(\vec{n})} T^{\mu\nu}, \tag{1.2}$$

where the massive gravitons are labeled by a $\delta$-dimensional vector of integers, $\vec{n} = (n_1, n_2, \ldots, n_\delta)$, $\bar{M}_{\mathrm{P}} = M_{\mathrm{P}}/\sqrt{8\pi} \sim 2.4 \times 10^{18}$ GeV is the reduced four-dimensional Planck scale, and $T_{\mu\nu}$ is the energy-momentum tensor of the SM fields. The Feynman rules that follow from Eq. (1.2) can be found in Refs. [5,7]. The individual KK resonances have masses equal to $m_{(\vec{n})} = |\vec{n}|/R$ and thus the mass gap between neighboring modes $\Delta m = R^{-1}$ is small for $\delta$ not too large. Quantitatively one finds $\Delta m \approx 20$ keV, 7 MeV and 0.1 GeV for $M_{\mathrm{S}} = 1$ TeV and $\delta = 4$, 6 and 8, respectively [5]. The discrete mass spectrum can thus be approximated by a continuum with a density of states $dN = \rho(m)dm$ [5,6], where

$$\rho(m) = S_{\delta-1} \frac{\bar{M}_{\mathrm{P}}^2}{M_{\mathrm{S}}^{2+\delta}} m^{\delta-1}, \quad \text{and} \quad S_{\delta-1} = \frac{2\pi^{\delta/2}}{\Gamma(\delta/2)}. \tag{1.3}$$

Inclusive collider cross sections, where one sums over all accessible KK modes, are obtained from a convolution of the cross section for an individual KK mode of mass $m$, $d\sigma_m$, with the mass density function $\rho(m)$ (1.3), $d\sigma/dm = \rho(m)d\sigma_m$. Although each individual graviton couples to SM matter with only gravitational strength $\propto 1/\bar{M}_{\mathrm{P}}$ [see Eq. (1.2)] and thus $d\sigma_m \propto 1/\bar{M}_{\mathrm{P}}^2$, inclusive collider processes are enhanced by the enormous number of accessible KK states $\propto \bar{M}_{\mathrm{P}}^2$ (1.3). The factors $\bar{M}_{\mathrm{P}}^2$ cancel in $d\sigma/dm = \rho(m)d\sigma_m$, leaving an overall suppression of only $M_{\mathrm{S}}^{-2-\delta}$. If the fundamental scale $M_{\mathrm{S}}$ is near the TeV-scale, graviton

 

production can thus be probed at present and future high-energy colliders.

Both virtual graviton exchange between SM particles and real graviton emission provide viable signatures of large extra dimensions at colliders. Since the coupling of gravitons with matter is suppressed $\propto 1/\bar{M}_{\rm P}$, direct graviton production gives rise to missing energy signals. Searches for graviton production have been performed in the processes $e^+e^- \to \gamma(Z) + E^{\rm miss}$ at LEP and $p\bar{p} \to \gamma(\text{jet}) + p_T^{\rm miss}$ at the Tevatron. The combined LEP limits [8] read $M_{\rm S} > 1.60, 1.20, 0.94, 0.77, 0.66$ TeV, for $\delta = 2, \cdots, 6$, respectively, while Tevatron searches exclude $M_{\rm S} > 1.40, 1.15, 1.04, 0.98, 0.94$ TeV, for $\delta = 2, \cdots, 6$, respectively [9,10]. Searches for the process $pp \to \text{jet} + p_T^{\rm miss}$ at the LHC will be able to extend the sensitivity to the fundamental scale $M_{\rm S}$ into the multi-TeV region [11–14].

Current analyses of graviton production at hadron colliders are based on LO cross sections, which are subject to large theoretical uncertainties from the choice of renormalization and factorization scales. In this paper we present the first calculation of the next-to-leading-order (NLO) QCD corrections to graviton production in the process $pp/p\bar{p} \to \text{jet} + G$ at hadron colliders, results for the QCD corrections in the photon channel have been presented in [15]. The NLO cross sections lead to significantly more accurate theoretical signal predictions and thereby more accurate constraints on $M_{\rm S}$ or, in the case of discovery, will allow to probe the model parameters. The NLO calculation also enables us to properly study the relative importance of multijet final states, which has been addressed in a recent calculation of the (tree-level) graviton plus di-jet cross section [16]. We note that NLO QCD corrections to the hadro-production of lepton and boson pairs in models with large extra dimensions have been presented in a series of recent papers [17,18].

The remainder of this paper is structured as follows: In Sec. II we present some details of the NLO QCD cross section calculation for $pp/p\bar{p} \to \text{jet} + G$. Numerical results for the Tevatron and the LHC are presented in Sec. III. We conclude in Sec. IV. More details of the calculation and selected formulae are presented in the Appendix.

## II. CALCULATION

The LO cross section for graviton plus jet production receives contributions from the partonic processes

$$q\bar{q} \to gG, \qquad qg \to qG \quad \text{and} \quad gg \to gG. \tag{2.1}$$

The relevant Feynman diagrams are depicted in Fig. 1. The LO partonic cross sections of the processes (2.1) have first been presented in Ref. [5]; the corresponding helicity amplitudes are discussed in the Appendix.

The NLO cross section consists of virtual corrections, real-emission contributions and a collinear term, which is a finite remainder of the factorization of collinear singularities into the parton distribution functions (PDFs). We use dimensional regularization [19] in $d = 4 - 2\epsilon$ dimensions to regulate the ultraviolet (UV) and infrared (IR) divergences, and apply the dipole subtraction scheme [20] to cancel the infrared singularities. The UV divergences are removed by renormalization of the QCD coupling $\alpha_s$ in the $\overline{\rm MS}$-scheme.

We have performed two independent calculations of the virtual corrections, described in more detail below, and have checked gauge invariance and Ward identities arising from general coordinate invariance; see Ref. [16] for more details. The numerical implementation of the real-emission contributions is based on MADGRAPH [21] and MADDIPOLE [22]. Some details of the NLO calculation are provided below.

### A. Virtual corrections

The virtual corrections to $pp/p\bar{p} \to \text{jet} + G$ arise from the interference of the Born and one-loop amplitudes. Example one-loop Feynman diagrams are depicted in Fig. 2. The Feynman rules for the graviton interaction

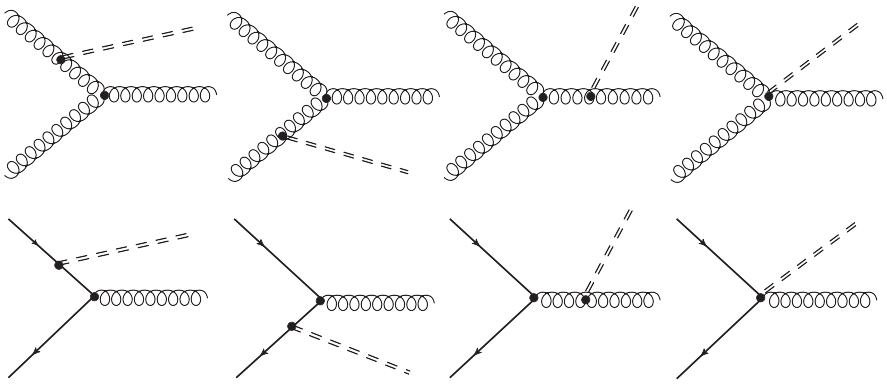

FIG. 1. The LO Feynman diagrams for $gg, q\bar{q} \to G + \text{jet}$. The $gq$ channel is related to the $q\bar{q}$ channel by crossing and not shown.

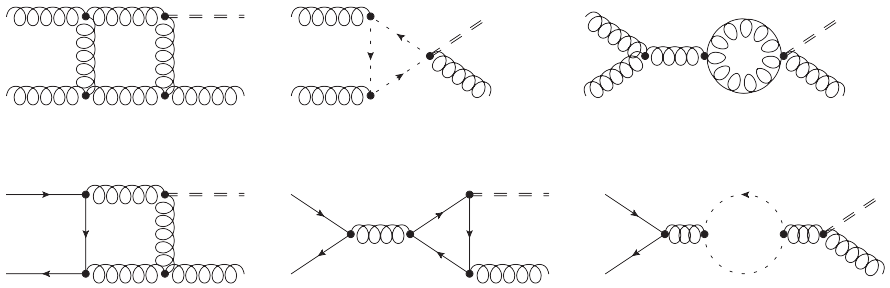

FIG. 2. Examples of NLO QCD virtual Feynman diagrams for $pp \to G +$ jet. The dotted loops represent ghost particles.

with the SM fields can be found in Refs. [5,7,17].[1] For external gluons we choose the light-cone gauge to avoid introducing external ghost lines, as in the HELAS convention [23]. The internal gluon propagators are evaluated in the 't Hooft-Feynman gauge, and the unphysical degrees of freedom are canceled by ghost loops. The UV poles are removed by $\overline{\text{MS}}$-renormalization of $\alpha_s$, while the IR singularities cancel against those from the real-emission contribution [see Eq. (2.2) below].

Two independent calculations are performed for the virtual corrections. The first calculation is based on the MATHEMATICA package FEYNCALC [24]. Because of the Lorentz indices of the spin-2 graviton, we encounter high-rank tensor integrals, such as rank-5 4-point functions. Special care is taken to reduce those to one-loop scalar integrals by an independent MATHEMATICA code, following the prescription of Ref. [25].

In the second calculation, the one-loop diagrams are generated with QGRAF [26] and then projected onto helicity components and amplitude coefficients with FORM [27]. Details of the projection are given in the Appendix and can also be found in Ref. [28], where the same method has been used. The tensor reduction is performed according to the GOLEM [29,30] reduction algorithm, supplemented with additional tensor reduction routines for rank $N+1$ $N$-point tensor integrals with $N \leq 3$. To calculate numerical results we employed the OMNICOMP-DVEGAS package [31], which facilitates parallelized adaptive Monte Carlo integration and was developed in the context of Ref. [32].

### B. Real-Emission contributions

The real-emission contribution comprises the radiation of a real gluon or a massless (anti-)quark. Soft and collinear singularities are isolated using dipole subtraction [20]. Collinear emission from initial state partons is factorized into the parton distribution functions defined in the $\overline{\text{MS}}$-scheme. The remaining IR and IR/collinear singularities, which cancel those of the virtual corrections, read in the notation of [20]

$$\langle I(\epsilon)\rangle_{gg} = \frac{\alpha_s}{2\pi}\frac{(4\pi\mu^2)^\epsilon}{\Gamma(1-\epsilon)}\left\{\frac{3\beta_0}{2\epsilon} + \frac{C_A}{\epsilon^2}[(s)^{-\epsilon} + (-t)^{-\epsilon} + (-u)^{-\epsilon}]\right\}|\mathcal{M}^{\text{B}}_{gg}|^2, \tag{2.2}$$

$$\langle I(\epsilon)\rangle_{q\bar{q}} = \frac{\alpha_s}{2\pi}\frac{(4\pi\mu^2)^\epsilon}{\Gamma(1-\epsilon)}\left\{\frac{\beta_0}{2\epsilon} + \frac{3C_F}{2\epsilon} + \frac{C_A}{\epsilon^2}[(-t)^{-\epsilon} + (-u)^{-\epsilon}] + \frac{(-C_A+2C_F)}{\epsilon^2}(s)^{-\epsilon}\right\}|\mathcal{M}^{\text{B}}_{q\bar{q}}|^2, \tag{2.3}$$

where $s$, $t$, and $u$ are the Mandelstam variables, $\beta_0 = (11C_A - 4n_f T_R)/3$ with $n_f = 5$, and $\langle I(\epsilon)\rangle_{gq}$ can be obtained by crossing from $\langle I(\epsilon)\rangle_{q\bar{q}}$.

The real-emission matrix elements and subtraction terms are generated with MADGRAPH with spin-2 particles [21] and MADDIPOLE [22], respectively, and are implemented in a parton-level Monte Carlo program.

## III. NUMERICAL RESULTS

In this section we present NLO cross sections for $pp/p\bar{p} \to$ jet $+ G$ at the Tevatron ($\sqrt{S} = 1.96$ TeV) and the LHC ($\sqrt{S} = 14$ TeV). Before we proceed with the numerical results, we note that the interaction of the KK gravitons with SM matter is described by an effective theory [5–7], which is valid only for scattering energies $\sqrt{\hat{s}}$ smaller than the fundamental scale $M_S$. While hadron collider cross sections in principle involve partonic scatterings with energies $\sqrt{\hat{s}}$ up to the collider energy $\sqrt{S}$, the rapid decrease of the parton luminosities at large $\sqrt{\hat{s}}$ suppresses the high-energy region and allows for a cross section prediction that is not very sensitive to the UV completion of the effective theory. We will return to this issue at the end of the section and provide quantitative estimates of the UV sensitivity of the theoretical prediction.

The numerical results presented below are obtained with $\alpha_s$ and the parton distribution functions defined in the $\overline{\text{MS}}$-scheme, with five active flavours. Throughout our calculation, we employ the 2008 MSTW LO(NLO) PDF [33] at LO(NLO), with the corresponding value for the

[1]Note that there are different sign conventions in the definition of the covariant derivative, which leads to a sign difference in the Feynman rules for 4-point vertices such as $VVVG$.

strong coupling $\alpha_s$. Our default choice for the renormalization and factorization scale is the transverse momentum of the graviton, $\mu = P_T^G$.

To suppress SM backgrounds in the LHC graviton searches [11], we require

$$P_T^{\rm miss} > 500 \text{ GeV}. \tag{3.1}$$

The jets are defined by the $k_T$ algorithm, with the resolution parameter set to $D = 0.6$, and are required to satisfy $|\eta_j| < 4.5$ and $P_T^j > 50$ GeV.

For the Tevatron predictions we use the same settings as in the recent CDF study [9], i.e.

$$P_T^{\rm miss} > 120 \text{ GeV}, \qquad P_T^j > 150 \text{ GeV}, \quad \text{and} \quad |\eta_j| < 1. \tag{3.2}$$

Also here, jets are defined by the $k_T$ algorithm with $D = 0.7$, and are required to satisfy $|\eta_j| < 3.6$ and $P_T^j > 20$ GeV. A second jet with $P_T > 60$ GeV is vetoed. We will, however, also discuss results without the jet veto.

We first focus on the scale dependence of the total cross section. For illustration, we set the model parameters to $\delta = 4$, and $M_{\rm S} = 5$ TeV (LHC) and 1 TeV (Tevatron). Note that the cross section scales as $\sigma \propto M_{\rm S}^{-2-\delta}$ so that results for other values of $M_{\rm S}$ can be obtained by rescaling our predictions. Unfortunately, it is not possible to determine both $M_{\rm S}$ and $\delta$ independently from just the shape of the $P_T^{\rm miss}$ spectrum [11]. To resolve these parameters would need very accurate measurements at different hadron collider center-of-mass energies; the ratio of graviton production cross sections at different center-of-mass energies depends on $\delta$ through the kinematic limit on the graviton mass, while the dependence on $M_{\rm S}$ cancels. Operating the LHC at 7 TeV and 14 TeV center-of-mass energies may offer such an opportunity. We impose the kinematical cuts listed in Eqs. (3.1) and (3.2) for the LHC and the Tevatron, respectively. The LO and NLO results are shown in Fig. 3 as a function of the renormalization and factorization scales varied around the central scale $\mu = P_T^G$. We observe that the scale dependence of the NLO cross section is significantly smaller than that of the LO cross section, both at the LHC and at the Tevatron: changing $\mu$ in the range between $P_T^G/2$ and $2P_T^G$, the LO cross section varies by $\approx 30\%$, while the scale uncertainty at NLO is less than $\approx 10\%$. We have also varied both scales independently and find that in all cases the NLO uncertainty is less than approximately 10%. At the LHC, the $K$-factor, $K = \sigma_{\rm NLO}/\sigma_{\rm LO}$, is sizeable and positive at the central scale $\mu = P_T^G$, increasing the LO cross section prediction by about 20%. At the Tevatron, the QCD corrections are mild near $\mu = P_T^G$ with $K \approx 1$, but are essential to reduce the theoretical uncertainty.

The experimental analyses at the LHC and the Tevatron rely on the $P_T^{\rm miss}$ and $P_T^{\rm jet}$ distributions, respectively. In Figs. 4 and 5 we show the scale dependence of these

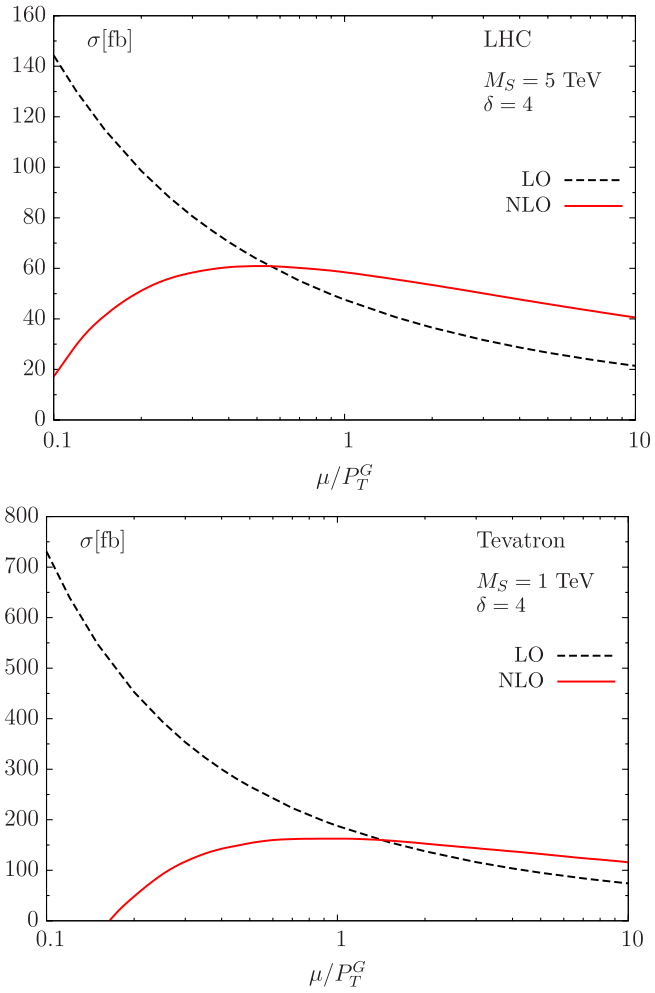


FIG. 3 (color online). Scale variation for the integrated cross section at LHC and Tevatron, for a common scale $\mu = \mu_r = \mu_f$. Selection cuts are described in the text.

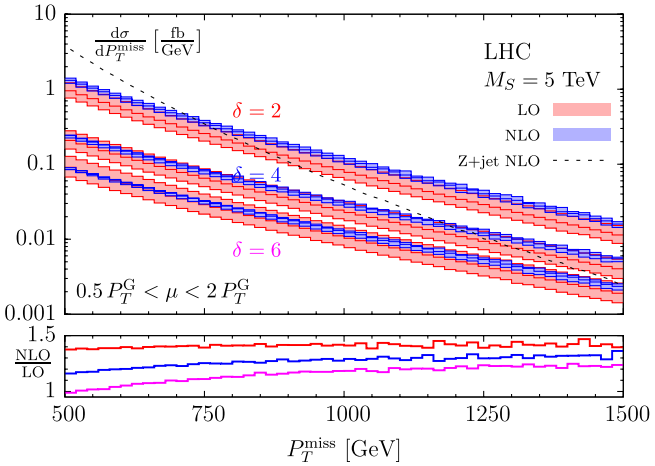


FIG. 4 (color online). $P_T^{\rm miss}$ distribution for the graviton signal at the LHC with scale uncertainty bands ($0.5P_T^G < \mu < 2P_T^G$). Also given is the NLO distribution for the dominant $Z \to \nu\bar{\nu}$ background. The lower part of the plot shows $K(P_T) = (d\sigma_{\rm NLO}/dP_T)/(d\sigma_{\rm LO}/dP_T)$ for $\delta = 2$, 4, 6 (top down).

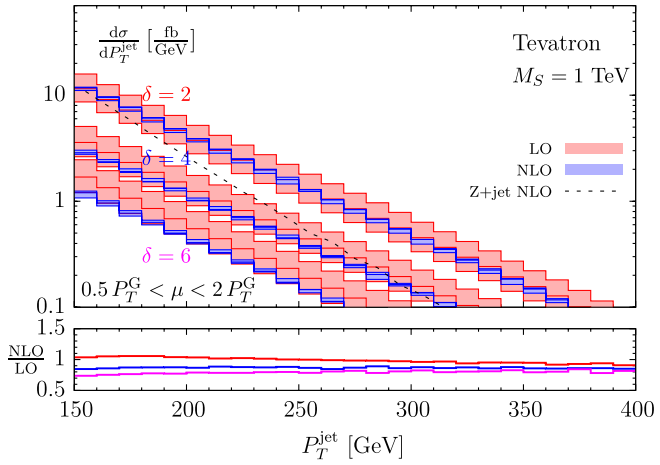


FIG. 5 (color online). Same as Fig. 4 but for the $P_T$ distribution of the leading jet at the Tevatron.

distributions, for different choices of the number of extra dimensions $\delta = 2, 4, 6$. Current Tevatron limits appear to exclude $M_S = 1$ TeV for $\delta < 4$. However, these analyses are based on leading-order predictions and should be refined using the NLO results presented here. We thus include numerical predictions for $M_S = 1$ TeV and $\delta = 2, 4, 6$ below. We also show the NLO QCD predictions for the main background $pp \to Z(\to \nu\bar{\nu}) + \text{jet}$ obtained with MCFM [34]. [Note that establishing an excess in graviton plus jet production at hadron colliders requires an excellent experimental understanding of the SM background. To precisely estimate the dominant $pp \to Z(\to \nu\bar{\nu}) + \text{jet}$ background process one can rely on a calibration sample of the related process $pp \to Z(\to e^+e^-/\mu^+\mu^-) + \text{jet}$ [9–11,13]. Furthermore, the signal to background ratio can be improved by increasing the $P_T^{\text{miss}}$- cut.] The bands show the uncertainty of the LO and NLO predictions when varying the renormalization and factorization scales in the range $P_T^G/2 < \mu < 2P_T^G$. The reduction of the scale uncertainty at NLO is evident. Figures 4 and 5 also display the $P_T$ dependence of the $K$ factors, defined as $K(P_T) = (d\sigma_{\text{NLO}}/dP_T)/(d\sigma_{\text{LO}}/dP_T)$. The $K$ factors are sizeable at the LHC (Fig. 4), as noted before, increasing with decreasing $\delta$. Furthermore, the $K$ factors depend on the kinematics and increase with increasing $P_T^{\text{miss}}$. At the Tevatron, the $K$ factors are in general near or below one and only mildly depend on the jet transverse momentum; see Fig. 5.

We have also investigated the uncertainty of the NLO cross section prediction due to the parton distribution function. Using the MSTW error PDFs [33], we find an uncertainty of less than approximately 15% for graviton production at the LHC, even for large $P_T^{\text{miss}} > 1$ TeV. At the Tevatron, the uncertainty is even smaller and approximately 5%.

Let us now examine the contribution of the real-emission cross section with two hard jets. In Fig. 6 we

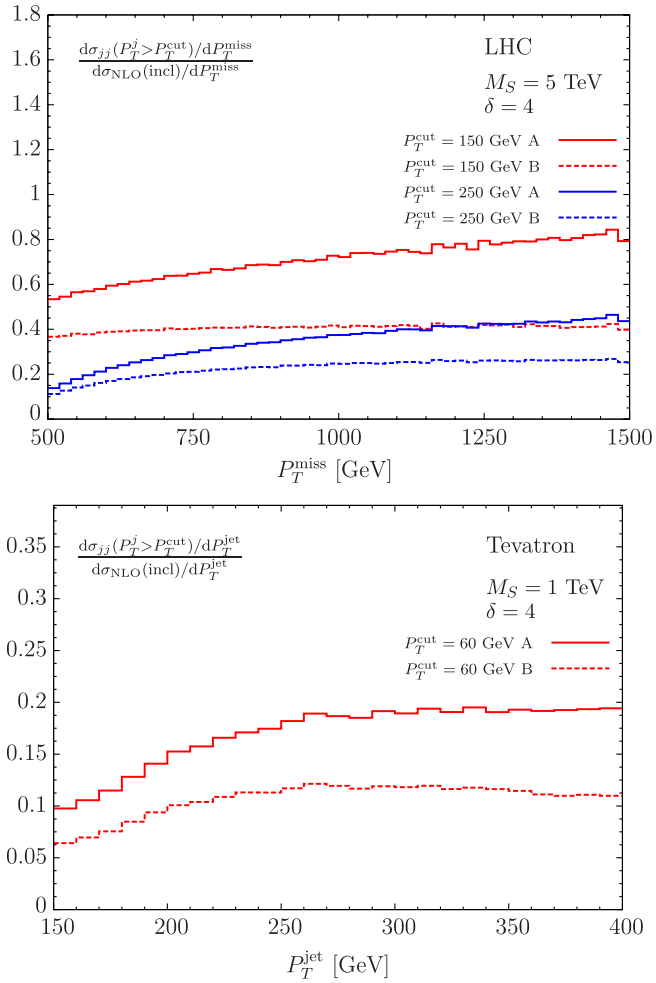


FIG. 6 (color online). Di-jet fraction of graviton plus jets events at the LHC and Tevatron. Results are given for the two scale choices $\mu = p_T^G$ and Eq. (3.3), respectively, and minimal transverse momentum requirements $P_T^{\text{cut}}$ for the second jet.

show the ratio of the cross section where we require two hard jets with $P_T^j > P_T^{\text{cut}}$ and the inclusive cross section, as a function of $P_T^{\text{miss}}$ and the leading $P_T^{\text{jet}}$ at the LHC and the Tevatron, respectively. Results are presented for the minimum jet-$P_T$ set to $P_T^{\text{cut}} = 150$ GeV and 250 GeV for the LHC, and $P_T^{\text{cut}} = 60$ GeV for the Tevatron. Moreover, in Fig. 6, we show results with an alternative choice of settings (labeled B in the plot) defined as

$$\mu_f = \min(P_T^j) \quad \text{and} \quad \alpha_s = \sqrt{\alpha_s(P_T^{j_1})\alpha_s(P_T^{j_2})}, \tag{3.3}$$

which was used in Ref. [16] for the real-emission contribution with two hard jets. We observe that the fraction of events containing two jets with $P_T^j > 250$ GeV is 20–40% at the LHC for $P_T^{\text{miss}}$ above 1 TeV, depending on the choice of input parameters for the 2-jet contribution. Between 40% and 70% of the events with $P_T^{\text{miss}} > 1$ TeV contain two jets with $P_T^j > 150$ GeV. We note that even for the scale choice B, as given in Eq. (3.3), the fraction of di-jet

events is smaller than estimated in Ref. [16]. This is due to the denominator, i.e. the larger inclusive cross section as predicted at NLO. Nevertheless, also with our new estimate we expect a large fraction of high $P_T^{\rm miss}$ events with two or more hard jets at the LHC. While the quantitative estimates given in Ref. [16] are thus changed due to the impact of the NLO corrections, the qualitative conclusions remain valid. At the Tevatron, the contribution of 2-jet events with $P_T^j >$ 60 GeV is moderate and does not exceed 20%. The difference between the results with the two different scale settings, which represent part of the uncertainty for the (tree-level) 2-jet cross section, increases with increasing $P_T$, as the difference between our default choice of scale and $\alpha_s$ and the alternative choice (3.3) becomes larger.

As mentioned at the beginning of this section, the results of the effective field theory calculation are valid only as long as the scales involved in the hard scattering process do not exceed the fundamental scale $M_{\rm S}$. To quantify the sensitivity of our prediction to the unknown UV completion of the theory, we compare our NLO results with those involving a truncation scheme which sets the cross section to zero if $Q_{\rm truncation} \geq M_{\rm S}$. In the numerical results presented below, the truncation parameter $Q_{\rm truncation}$ is taken to be the invariant mass of the missing momentum and observable jet(s),

$$Q_{\rm truncation} = |P^G + P^{\rm jet(s)}|. \tag{3.4}$$

This definition is equal to $Q_{\rm truncation} = \sqrt{\hat{s}}$ at LO, but takes into account that the effective partonic energy of the scattering process can be reduced by collinear initial state radiation at NLO and thus provides an IR-safe definition of the truncation parameter. NLO results for the transverse momentum distributions with and without the hard truncation scheme for $\delta = 2, 4, 6$ at the LHC and the Tevatron are shown in Figs. 7 and 8, respectively. As expected, the differences between the two calculations increase with increasing $\delta$, as the average graviton mass is shifted to larger values. Also, the differences become larger as $P_T^{\rm miss}(P_T^{\rm jet})$ increase. For example, for the LHC, at $P_T^{\rm miss} =$ 1250 GeV, the uncertainties for $\delta = 2, 4, 6$ are about 5%, 20%, and 50%, respectively, while for the Tevatron, at $P_T^{\rm jet} = 250$ GeV, the uncertainties for $\delta = 2, 4, 6$ are about 2%, 10%, and 25%. Note that the results with the hard truncation do not obey the simple scaling $\sigma \propto M_{\rm S}^{-2-\delta}$.

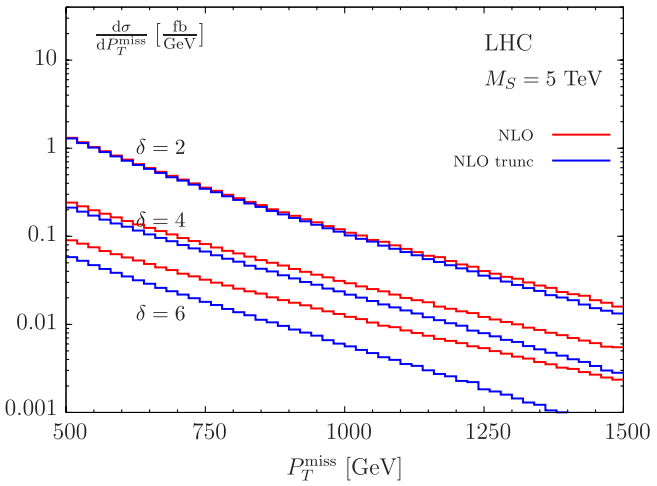


FIG. 7 (color online). Effect of truncation of the partonic cross section above $Q_{\rm truncation} = M_{\rm S}$ at the LHC. See text for details.

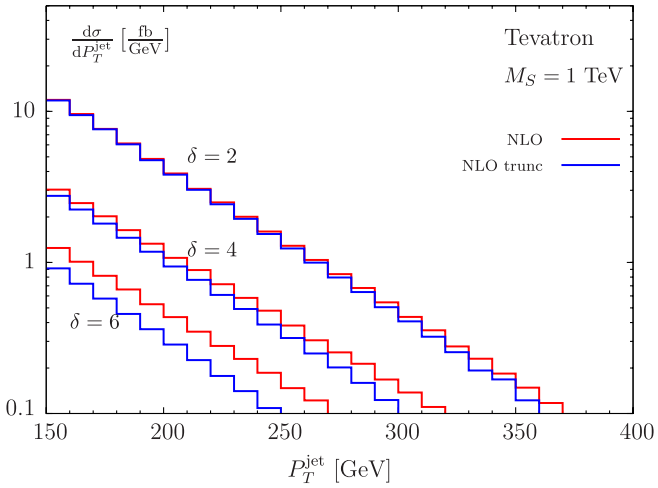


FIG. 8 (color online). Effect of truncation of the partonic cross section above $Q_{\rm truncation} = M_{\rm S}$ at the Tevatron. See text for details.

Finally, we comment on the prospects for graviton searches during the initial phase of the LHC operating at 7 TeV. Even at half the nominal center-of-mass energy, the LHC will be able to extend the sensitivity of current Tevatron searches to larger values of $M_{\rm S}$ [13,14]. For illustration we show in Fig. 9 the NLO $P_T^{\rm miss}$ distribution

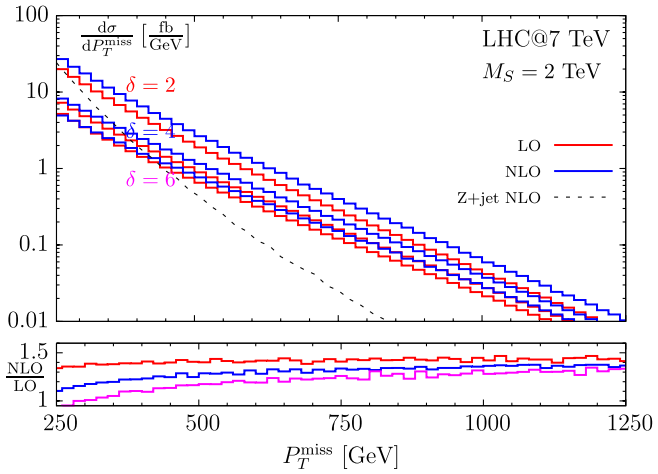


FIG. 9 (color online). $P_T^{\rm miss}$ distribution for the graviton signal at the LHC at 7 TeV cms energy. Also shown is the NLO distribution for the dominant $Z \to \nu\bar{\nu}$ background. The lower part of the plot shows $K(P_T) = (d\sigma_{\rm NLO}/dP_T)/(d\sigma_{\rm LO}/dP_T)$ for $\delta = 2, 4, 6$ (top down).

for $M_S = 2$ TeV and $\delta = 2, 4, 6$, together with the dominant SM background. We find sizeable signal rates, in particular, for $\delta = 2$, which exceed the background for $P_T^{\text{miss}} \gtrsim 250$ GeV. We reemphasize that comparing monojet signatures at 7 TeV with results obtained at higher center-of-mass energies during a later stage of LHC operation may allow to disentangle the fundamental parameters $M_S$ and $\delta$.

## IV. SUMMARY

We have presented the first calculation of the NLO QCD corrections to Kaluza-Klein graviton plus jet hadroproduction in models with large extra dimensions. The calculation has been set up as a fully flexible parton-level Monte Carlo program,[2] and results have been presented for cross sections and distributions at the Tevatron and at the LHC.

The QCD corrections stabilize the theoretical prediction and significantly reduce the scale uncertainty to a level of approximately 10%. Near the central scale, $\mu = P_T^G$, the QCD corrections increase the cross section at the LHC by 30–50%, depending on the kinematical region and the choice of model parameters. At the Tevatron, the QCD corrections are modest and negative near $\mu = P_T^G$ and do not strongly depend on the kinematics. A significant contribution of di-jet events is expected at the LHC, where 20–40% of signal events at $P_T^{\text{miss}} > 1$ TeV contain two jets with $P_T^j > 250$ GeV. At the Tevatron, on the other hand, the contribution of 2-jet events with $P_T^j > 60$ GeV is moderate and does not exceed 20%. The theoretical uncertainty of the cross section prediction due to the parton distribution functions is mild, with approximately 15% and 5% at the LHC and the Tevatron, respectively.

We have also studied the uncertainties arising from the UV completion of the theory by comparing our default NLO results with those involving a hard truncation scheme. The differences between the two calculations are small for $\delta = 2$ but can reach up to 50% for $\delta = 6$ and large $P_T$. Reducing these uncertainties requires to go beyond the effective field theory approximation of Eq. (1.2), which is beyond the scope of the present paper. Ignoring form factor effects for the graviton couplings to gluons and quarks and ignoring Kaluza-Klein excitations in the loops, defines one particular phenomenological model. For this model, our calculation quantifies the size of QCD corrections, and these results may then be taken as an indication of what to expect of QCD corrections in more complete models of the UV physics.

## ACKNOWLEDGMENTS

This work is supported in part by the Deutsche Forschungsgemeinschaft under Grant No. SFB/TR-9 "Computergestützte Theoretische Teilchenphysik," the Helmholtz Alliance "Physics at the Terascale," and the European Community's Marie-Curie Research Training Network under Contract No. MRTN-CT-2006-035505 "Tools and Precision Calculations for Physics Discoveries at Colliders." S. K. is grateful to Thomas Binoth and Nikolas Kauer for valuable discussions. S. K. and M. K. would like to thank Arnd Meyer for discussions on experimental aspects of monojet searches.

## APPENDIX: AMPLITUDE CALCULATION

The amplitude for the partonic processes $gg \to G + \text{jet}$ and $q\bar{q} \to G + \text{jet}$ can be expressed as

$$\begin{aligned}\mathcal{M}(g(p_1,\lambda_1)g(p_2,\lambda_2) &\to g(p_3,\lambda_3)G(p_4,\lambda_4)) \\ &= \mathcal{M}^{\mu_1\mu_2\mu_3\mu\nu}\epsilon_{\mu_1}^{\lambda_1}\epsilon_{\mu_2}^{\lambda_2}\epsilon_{\mu_3}^{\lambda_3}\epsilon_{\mu\nu}^{\lambda_4}f^{abc}, \\ \mathcal{M}(q(p_1,\lambda_1)\bar{q}(p_2,\lambda_2) &\to g(p_3,\lambda_3)G(p_4,\lambda_4)) \\ &= \langle p_2^{\lambda_2}|\mathcal{M}^{\mu_3\mu\nu}|p_1^{\lambda_1}\rangle\epsilon_{\mu_3}^{\lambda_3}\epsilon_{\mu\nu}^{\lambda_4}T_{ij}^a,\end{aligned} \tag{A1}$$

where $|p_i^{\pm}\rangle$ is the Weyl spinor for a massless particle with momentum $p_i$. Since we consider all quarks to be massless, the helicity of the quark line is conserved, and therefore we have $\lambda_1 = \lambda_2 \in [+, -]$. (Note that the physical helicity of the antiquark is given by $-\lambda_2$.)

Applying spinor helicity methods [35], the polarization vector for a massless spin-1 boson for helicity $\pm$ is given by

$$\epsilon_\mu^{\pm}(p, r) = \pm\frac{\langle r^{\mp}|\gamma_\mu|p^{\pm}\rangle}{\sqrt{2}\langle r^{\mp}|p^{\pm}\rangle}, \tag{A2}$$

where the vector $r$ in (A2) denotes an arbitrary reference vector (with $r^2 = 0$).

The polarization tensor $\epsilon_{\mu\nu}^{\lambda_4}$ of the graviton, a massive spin-2 vector boson, can be constructed from the polarization vectors of massive spin-1 bosons, $\epsilon_\mu^{\pm,0}$, as follows[3]:

$$\begin{aligned}\epsilon_{\mu\nu}^{++} &= \epsilon_\mu^+\epsilon_\nu^+, \\ \epsilon_{\mu\nu}^{+} &= \frac{1}{\sqrt{2}}(\epsilon_\mu^+\epsilon_\nu^0 + \epsilon_\mu^0\epsilon_\nu^+), \\ \epsilon_{\mu\nu}^{0} &= \frac{1}{\sqrt{6}}(\epsilon_\mu^+\epsilon_\nu^- + \epsilon_\mu^-\epsilon_\nu^+ - 2\epsilon_\mu^0\epsilon_\nu^0), \\ \epsilon_{\mu\nu}^{--} &= \epsilon_\mu^-\epsilon_\nu^-, \\ \epsilon_{\mu\nu}^{-} &= \frac{1}{\sqrt{2}}(\epsilon_\mu^-\epsilon_\nu^0 + \epsilon_\mu^0\epsilon_\nu^-).\end{aligned} \tag{A3}$$

In order to extend the spinor-formalism to massive gauge bosons, it is useful to decompose the graviton mo-

[2]The FORTRAN code is available upon request from karg@physik.rwth-aachen.de.

[3]Note that Eq. (A2) follows the convention $\epsilon_\mu^{\lambda,*} = +\epsilon_\mu^{-\lambda}$. An additional sign is sometimes included in the literature, which would alter the sign of the third term in $\epsilon_{\mu\nu}^0$ in Eq. (A3).

mentum into two lightlike vectors:

$$p_4 = q_4 + \alpha r, \quad \text{with} \quad p_4^2 = m^2,$$
$$q_4^2 = 0 = r^2, \qquad \alpha = \frac{m^2}{2p_4 \cdot r}, \tag{A4}$$

where the arbitrary reference momentum $r$ can be taken from the list of available lightlike external momenta. The expressions for the three polarization vectors $\epsilon^{\pm,0}$ can now be constructed from the two lightlike vectors $p_4$ and $r$ and read

$$\epsilon_\mu^\pm(p_4, m) = \pm \frac{\langle r^\mp | \gamma_\mu | q_4^\pm \rangle}{\sqrt{2}\langle r^\mp | p^\pm \rangle},$$
$$\epsilon_\mu^0(p_4, m) = \frac{1}{m}(q_4^\mu - \alpha r^\mu). \tag{A5}$$

Of course, individual helicity amplitudes are no longer independent of the choice of the reference momentum of the graviton. However, we are only interested in the spin *sum*, which is independent of the reference momentum.

By a suitable choice of the reference vectors, we can assemble the individual spinor products and write them as a trace times a global spinorial factor. The projector for the $\lambda_1\lambda_2\lambda_3 = + + +$ helicity combination, for example, reads

$$\epsilon^+_{\mu_1}\epsilon^+_{\mu_2}\epsilon^+_{\mu_3} = \frac{\langle 3^-|\mu_1|1^-\rangle}{\sqrt{2}\langle 31\rangle}\frac{\langle 1^-|\mu_2|2^-\rangle}{\sqrt{2}\langle 12\rangle}\frac{\langle 2^-|\mu_3|3^-\rangle}{\sqrt{2}\langle 23\rangle}$$
$$= \frac{\mathrm{tr}[(1-\gamma_5)3\mu_1 1\mu_2 2\mu_3]}{4\sqrt{2}\langle 31\rangle\langle 12\rangle\langle 23\rangle}, \tag{A6}$$

and the projector for the $\lambda_4 = 2+$ helicity is given by

$$\epsilon^{++}_{\mu\nu} = \frac{\langle 1^-|\mu|4^-\rangle}{\sqrt{2}\langle 14\rangle}\frac{\langle 4^-|\not{p}_2|1^-\rangle}{\langle 42\rangle[21]}\frac{\langle 1^-|\nu|4^-\rangle}{\sqrt{2}\langle 14\rangle}\frac{\langle 4^-|\not{p}_2|1^-\rangle}{\langle 42\rangle[21]}$$
$$= \frac{\mathrm{tr}[(1-\gamma_5)1\mu 421\nu 42]}{4\langle 14\rangle^2\langle 42\rangle^2[21]^2}, \tag{A7}$$

with the spinor inner products $\langle ij\rangle = \langle p_i^-|p_j^+\rangle$, $[ij] = \langle p_i^+|p_j^-\rangle$.

Note that the 40 (20) helicities for $gg \to gG(q\bar{q} \to gG)$ are related to each other by discrete symmetries, like parity, Bose symmetry or invariance under charge conjugation. The symmetries therefore allow for a cross check of the results or can be used to reduce the algebraical work by calculating only a generic set of helicity amplitudes. In this way, we could perform the spin sum by computing only 1 (2) helicity amplitude(s) for $gg \to gG(q\bar{q} \to gG)$.

The helicity amplitudes for $gg \to gG$ and $q\bar{q} \to gG$ summed over the polarization of the graviton are given by

$$\sum_{\lambda_4} |\mathcal{M}^{+--\lambda_4}_{gg\to gG}|^2 = \frac{2\hat{u}^4}{stu} \quad \text{and}$$
$$\sum_{\lambda_4} |\mathcal{M}^{---\lambda_4}_{q\bar{q}\to gG}|^2 = \frac{\hat{u}^2}{2stu}(4tu + sm_G^2), \tag{A8}$$

where $\hat{u} = u - m_G^2$ etc. Applying Bose and parity transformations on the above expressions gives us all helicity amplitudes.

Summing over final colors and averaging over initial helicities and colors, the squared LO matrix elements are given by

$$|\mathcal{M}_{\mathrm{LO}}|^2(gg \to gG) = \frac{3}{32}\frac{g_s^2}{\bar{M}_{\mathrm{P}}^2}\left(4\frac{\hat{s}^4 + \hat{t}^4 + \hat{u}^4}{stu}\right),$$
$$|\mathcal{M}_{\mathrm{LO}}|^2(q\bar{q} \to gG) = \frac{1}{9}\frac{g_s^2}{\bar{M}_{\mathrm{P}}^2}\left((4tu + sm_G^2)\frac{\hat{t}^2 + \hat{u}^2}{stu}\right), \tag{A9}$$

in agreement with [5], but in a form where the symmetries are more obvious. The process $qg \to qG$ is related by crossing to $q\bar{q} \to gG$.


[1] See e.g. C. Amsler *et al.* (Particle Data Group), Phys. Lett. B **667**, 1 (2008).

[2] N. Arkani-Hamed, S. Dimopoulos, and G. Dvali, Phys. Lett. B **429**, 263 (1998); **436**, 257 (1998); Phys. Rev. D **59**, 086004 (1999).

[3] D. J. Kapner, T. S. Cook, E. G. Adelberger, J. H. Gundlach, B. R. Heckel, C. D. Hoyle, and H. E. Swanson, Phys. Rev. Lett. **98**, 021101 (2007).

[4] See e.g. N. Kaloper, J. March-Russell, G. D. Starkman, and M. Trodden, Phys. Rev. Lett. **85**, 928 (2000); K. R. Dienes and A. Mafi, Phys. Rev. Lett. **88**, 111602 (2002); G. F. Giudice, T. Plehn, and A. Strumia, Nucl. Phys. **B706**, 455 (2005).

[5] G. F. Giudice, R. Rattazzi, and J. D. Wells, Nucl. Phys. **B544**, 3 (1999).

[6] E. A. Mirabelli, M. Perelstein, and M. E. Peskin, Phys. Rev. Lett. **82**, 2236 (1999).

[7] T. Han, J. D. Lykken, and R. J. Zhang, Phys. Rev. D **59**, 105006 (1999).

[8] LEP Exotica Working Group, Report No. 2004-03, 2004.

[9] T. Aaltonen *et al.* (CDF Collaboration), Phys. Rev. Lett. **101**, 181602 (2008).

[10] V. M. Abazov *et al.* (D0 Collaboration), Phys. Rev. Lett. **101**, 011601 (2008).

[11] L. Vacavant and I. Hinchliffe, J. Phys. G **27**, 1839 (2001).

[12] X. G. Wu and Z. Y. Fang, Phys. Rev. D **78**, 094002 (2008).

[13] CMS Collaboration, Report No. CMS-PAS-EXO-09-013, 2009.
[14] CMS Collaboration, CMS Note No. 2010/008, 2010.
[15] X. Gao, C. S. Li, J. Gao, J. Wang, and R. J. Oakes, Phys. Rev. D **81**, 036008 (2010).
[16] K. Hagiwara, P. Konar, Q. Li, K. Mawatari, and D. Zeppenfeld, J. High Energy Phys. 04 (2008) 019.
[17] P. Mathews, V. Ravindran, K. Sridhar, and W. L. van Neerven, Nucl. Phys. **B713**, 333 (2005).
[18] M. C. Kumar, P. Mathews, V. Ravindran, and A. Tripathi, Phys. Lett. B **672**, 45 (2009); Nucl. Phys. **B818**, 28 (2009); N. Agarwal, V. Ravindran, V. K. Tiwari, and A. Tripathi, Nucl. Phys. **B830**, 248 (2010); N. Agarwal, V. Ravindran, V. K. Tiwari, and A. Tripathi, arXiv:1003.5450.
[19] G. 't Hooft, M. J. G. Veltman, Nucl. Phys. **B44**, 189 (1972).
[20] S. Catani and M. H. Seymour, Nucl. Phys. **B485**, 291 (1997); **B510**, 503(E) (1998).
[21] K. Hagiwara, J. Kanzaki, Q. Li, and K. Mawatari, Eur. Phys. J. C **56**, 435 (2008).
[22] R. Frederix, T. Gehrmann, and N. Greiner, J. High Energy Phys. 09 (2008) 122.
[23] H. Murayama, I. Watanabe, and K. Hagiwara, KEK Report No. 91-11, 1992.
[24] R. Mertig, M. Bohm, and A. Denner, Comput. Phys. Commun. **64**, 345 (1991).
[25] A. Denner and S. Dittmaier, Nucl. Phys. **B658**, 175 (2003).
[26] P. Nogueira, J. Comput. Phys. **105**, 279 (1993).
[27] J. A. M. Vermaseren, arXiv:math-ph/0010025.
[28] T. Binoth, S. Karg, N. Kauer, and R. Ruckl, Phys. Rev. D **74**, 113008 (2006); T. Binoth, T. Gleisberg, S. Karg, N. Kauer, and G. Sanguinetti, Phys. Lett. B **683**, 154 (2010).
[29] T. Binoth, J. P. Guillet, G. Heinrich, E. Pilon, and C. Schubert, J. High Energy Phys. 10 (2005) 015.
[30] T. Binoth, M. Ciccolini, and G. Heinrich, Nucl. Phys. B, Proc. Suppl. **157**, 48 (2006).
[31] http://hepsource.sf.net/dvegas.
[32] N. Kauer and D. Zeppenfeld, Phys. Rev. D **65**, 014021 (2001); N. Kauer, Phys. Rev. D **67**, 054013 (2003).
[33] A. D. Martin, W. J. Stirling, R. S. Thorne, and G. Watt, Eur. Phys. J. C **63**, 189 (2009); Eur. Phys. J. C **64**, 653 (2009).
[34] J. M. Campbell and R. K. Ellis, Phys. Rev. D **65**, 113007 (2002); see http://mcfm.fnal.gov.
[35] Z. Xu, D. H. Zhang, and L. Chang, Nucl. Phys. **B291**, 392 (1987).